

The electrical asymmetry effect in electronegative CF₄ capacitive RF plasmas operated in the striation mode

Xiao-Kun Wang^{1,2} , Ranna Masheyeva^{3,4} , Yong-Xin Liu^{1,*} , Peter Hartmann³, Julian Schulze^{1,2}  and Zoltán Donkó³ 

¹ Key Laboratory of Materials Modification by Laser, Ion, and Electron Beams (Ministry of Education), School of Physics, Dalian University of Technology, 116024 Dalian, People's Republic of China

² Chair of Applied Electrodynamics and Plasma Technology, Faculty of Electrical Engineering and Information Sciences, Ruhr University Bochum, 44801 Bochum, Germany

³ Institute for Solid State Physics and Optics, Wigner Research Centre for Physics, 1121 Budapest, Hungary

⁴ Research Institute of Experimental and Theoretical Physics, Al-Farabi Kazakh National University, 050040 Almaty, Kazakhstan

E-mail: yxliu129@dlut.edu.cn

Received 3 May 2023, revised 13 July 2023

Accepted for publication 2 August 2023

Published 14 August 2023



Abstract

The Electrical Asymmetry Effect (EAE) provides control of the mean ion energy at the electrodes of multi-frequency capacitively coupled radio frequency plasmas (CCP) by tuning the DC self-bias via adjusting the relative phase(s) between the consecutive driving harmonics. Depending on the electron power absorption mode, this phase control affects the ion flux in different ways. While it provides separate control of the mean ion energy and flux in the α -mode, limitations were found in the γ - and Drift-Ambipolar modes. In this work, based on experiments as well as kinetic simulations, the EAE is investigated in the striation-mode, which is present in electronegative CCPs driven by low frequencies. The discharge is operated in CF₄ and is driven by two consecutive harmonics (4/8 MHz). The simulation results are validated against measurements of the DC self-bias and the spatio-temporally resolved dynamics of energetic electrons. To include heavy particle induced secondary electron emission realistically, a new computationally assisted diagnostic is developed to determine the corresponding secondary electron emission coefficient from a comparison of the DC self-bias obtained experimentally and from the simulations. Based on the validated simulation results, the EAE is found to provide separate control of the mean ion energy and flux in the striation mode, while the axial charged particle density profiles and the number of striations change as a function of the relative phase. This is understood based on an analysis of the ionization dynamics.

Keywords: electrical asymmetry effect, striations, capacitively coupled plasma, particle in cell simulation, experimental plasma diagnostics

(Some figures may appear in colour only in the online journal)

* Author to whom any correspondence should be addressed.

1. Introduction

Low temperature capacitively coupled plasmas (CCPs) are widely used in modern plasma processing applications such as etching and deposition in the microelectronics industry [1, 2]. The use of plasma etching for patterning thin film layers for the manufacturing of integrated circuits is of increasing importance [3]. Such etch processes [4–6] typically use electronegative gases such as CF_4 , C_4F_8 , and SF_6 [7–9]. With the increase in complexity of such applications and the reduction of the minimum feature size of individual circuit elements, empirical methods fail and a detailed fundamental understanding of the plasma physics of such discharges is required as a basis for knowledge based plasma process development.

This requires detailed insights into the spatio-temporally resolved dynamics and power absorption of energetic electrons, which generate various process relevant particle species (electrons, ions, neutral radicals) through electron-neutral collisions and determine their fluxes to the wafer as well as their energy distributions. Previous works revealed various modes of electron power absorption and their consequences on plasma characteristics. CCPs in electropositive gases at low pressures and voltages typically operate in the α -mode, where ambipolar-/pressure-heating of electrons leads to the generation of energetic electron beams at each electrode during the local sheath expansion [10–14]. In asymmetric discharges, non-linear Plasma Series Resonance oscillations of the radio frequency (RF) current can be self-excited and affect this mode via non-linear electron resonance heating of electrons [15–17]. Increasing the driving voltage, while keeping the neutral gas pressure low, can lead to a major contribution of electron induced secondary electrons to the ionization/dissociation dynamics, which are generated by the impact of energetic electrons at boundary surfaces [18, 19]. Increasing the pressure and/or voltage can induce a transition into the γ -mode, where heavy particles induce secondary electron emission from the electrodes. These electrons are accelerated into the plasma bulk by the sheath electric field, and multiply collisionally inside the sheaths creating avalanches of energetic electrons that contribute strongly to the ionization and dissociation [10, 20, 21]. Replacing the electropositive neutral gas by electronegative and/or reactive gases can induce a mode transition into the drift-ambipolar (DA) mode, in which electrons are accelerated by a strong drift electric field in the plasma bulk as a consequence of a low bulk conductivity and ambipolar fields at the sheath edges caused by local maxima of the electron density [22]. This behaviour arises as a consequence of the presence of negative ions and/or collisions. Mode transitions into the DA-mode have been studied as a function of the neutral gas pressure and driving voltage [22, 23]. Reducing the driving frequency in strongly electronegative CCPs, while the densities of positive and negative ions remain high, so that their plasma frequencies are similar to the driving frequency, was found to induce a mode transition into the striation mode [24]. In this mode, the positive and negative ions can react to the instantaneous bulk electric field and will, thus,

move into opposite directions at the times of high RF current within each RF period. This results in the formation of space charges, wherever density gradients are present, and ultimately in a striated pattern of regions of high and low electric field as well as plasma emission in the bulk. These self-organized striated structures have been studied as a function of the driving voltage amplitude and pressure in single frequency CCPs [25, 26] as well as in dual-frequency discharges driven at substantially different frequencies [27, 28]. Strong ion induced secondary electron emission from the electrodes was found to result in the disruption of the striations and to induce a mode transition into the γ -mode [29].

Based on such fundamental insights into the electron power absorption dynamics in CCPs, plasma control concepts can be developed and the limitations of their performance can be understood. One prominent example is the separate control of the mean ion energy and ion flux at the electrodes. Such separate control is essential, since the ion energy often determines chemical and physical processes at wafer/substrate surfaces, while the ion flux determines the process rates. In single frequency CCPs, such separate control cannot be achieved. In classical dual-frequency discharges driven by two significantly different frequencies, it is limited by the frequency coupling [30–33] and the effects of secondary electrons [20]. Such limitations can be overcome by voltage waveform tailoring (VWT) based on driving a CCP by multiple consecutive harmonics with individually adjustable phases and amplitudes [34–37]. The electrical asymmetry effect (EAE) was proposed to improve this separate control by driving the discharge by a fundamental frequency and its second harmonic [38, 39]. The mean energy of ions at each electrode can then be tuned nearly linearly by changing the phase angle between the driving harmonics. An analytical model was developed to understand the EAE and the improved quality of the separate control of the mean ion energy and flux via the EAE in electropositive CCPs operated in the α -mode [40], which was verified computationally [41] as well as experimentally [42–44] in Ar discharges driven at 13.56 MHz and 27.12 MHz. The EAE is based on the control of the DC self-bias by adjusting the relative phase between the driving harmonics, which, in turn, is a consequence of the phase control of the difference between the absolute values of the global extrema of the driving voltage waveform. In the α -mode, this phase control affects the electron power absorption dynamics in a way that results in an approximately constant ion flux because of the weak dependence of the period-averaged power dissipated to electrons on the phase angle [45, 46]. Similar results were obtained in weakly electronegative CCPs operated in O_2 [45, 47]. However, depending on the discharge conditions, limitations of the separate control of ion properties via the EAE were found. At low fundamental driving frequencies the control range of the DC self-bias accessible via phase control is reduced because of the charge dynamics [44]. Moreover, the electron power absorption mode was found to affect the quality of this separate control via the EAE. While it works well in the α -mode, limitations were found in the γ -mode due to the

detrimental effects of the ionization caused by secondary electrons on the plasma symmetry in the presence of the EAE [20]. Using different electrode materials characterized by different ion induced secondary electron emission coefficients (SEEC) was demonstrated to result in an enhanced control range of the mean ion energy based on a combination of the EAE with the secondary electron asymmetry effects [48, 49]. In strongly electronegative CCPs operated in CF_4 at 13.56 MHz and 27.12 MHz, the presence of the DA-mode was found to limit the separate control of ion flux and mean energy via the EAE due to a phase dependent electron power absorption and ionization caused by high bulk electric fields [50]. Further studies performed in electronegative gases such as SF_6/O_2 [51], CF_4 [52] and Cl_2 [53] also found a reduction of the control range of the DC self-bias and the mean ion energy via the EAE and a non-linear dependence of the DC self-bias on the relative phase between the driving harmonics due to high potential drop across the plasma bulk.

Despite the strong effects of the electron power absorption mode on the EAE, its performance has not been studied yet in the striation-mode. Therefore in this work, we investigate the EAE and the quality of the separate control of the mean ion energy and flux in electronegative CF_4 CCPs based on kinetic particle-in-cell simulations complemented with Monte Carlo treatment of collisions (PIC/MCC) and experiments. To ensure the presence of striations, the plasma is driven at low frequencies (4 MHz + 8 MHz) and is generated at a relatively high pressure of 100 Pa. Based on measurements of the DC self-bias and the spatio-temporally resolved dynamics of energetic electrons by Phase Resolved Optical Emission Spectroscopy (PROES), the simulation results are validated experimentally to ensure the accuracy of its results. In the frame of this experimental validation, the choice of the heavy particle induced SEEC is found to play a key role and a new computationally assisted diagnostic to determine this surface coefficient based on a comparison of the measured and computationally obtained DC self-bias is developed. It is based on the strong effect of ionization caused by such secondary electrons on the plasma symmetry [54]. Compared to previously developed computationally assisted diagnostic of SEECs, which require more complex PROES [55] and ion energy distribution function (IEDF) measurements [56], the new diagnostic is more simple and applicable in an industrial environment, since it only requires a voltage measurement experimentally. Based on this experimental validation and the heavy particle induced SEEC determined from this new diagnostic, the computational access to a variety of plasma parameters is used to analyze the performance of the EAE in the striation-mode. A good quality of the separate control of the ion flux and mean energy is found without detrimental effects of the striations as compared to CCPs operated in electronegative gases in the absence of striations. The axial charged particle density profile and the number of striations are, however, found to be affected by the phase control.

This paper is structured in the following way: in section 2, the experimental setup and all diagnostics are introduced as well as the PIC/MCC simulation used for the numerical

studies. The results are presented and discussed in section 3. Finally, conclusions are drawn in section 4.

2. Methods

2.1. Experimental setup

A schematic of the experimental setup including all diagnostics is shown in figure 1. The discharge is generated between two plane-parallel stainless steel electrodes having equal diameters of 10 cm and separated by a gap of $L = 1.5$ cm inside a cylindrical stainless-steel reactor (having an inner diameter of 40 cm), with electrically grounded walls. The space between the top (powered) electrode and the grounded chamber wall above this electrode is occupied by a Teflon block (shown in gray in the sketch of figure 1) to avoid the presence of parasitic discharges that could otherwise be generated in this region and would reduce the geometric reactor asymmetry. Additionally, both electrodes are surrounded by a cylindrical Teflon liner to confine the plasma radially to the volume in between the electrodes to ensure a good geometric reactor symmetry as the basis for comparisons of experimental results to those obtained from 1d3v PIC/MCC simulations, that inherently assume such a symmetry. Note that there is about -23 V DC self-bias under single frequency operation at 8 MHz with an amplitude of 301.7 V, which was neglected in the simulation. The top electrode includes a showerhead for the gas inlet as indicated by the dashed horizontal line. More detailed information on the reactor design can be found in our previous work [28].

A two-channel RF signal generator (Tektronix AFG31252) is used to generate low amplitude and phase-locked sinusoidal voltage waveforms at $f = 4$ MHz and its second harmonic (8 MHz). Each signal is amplified by a separate amplifier (AR, Model 1000A225) and applied to the top electrode through separate single frequency impedance matchings, i.e. the parallel impedance matching concept for multi-frequency CCPs is used [57]. Each matching branch is protected by an electrical filter (low- and high-pass) to prevent parasitic coupling between the matching branches. Ultimately, a voltage waveform, $\phi(t)$, of the following type is applied to the top electrode:

$$\phi(t) = \phi_0(\cos(2\pi ft + \theta) + \cos(4\pi ft)). \quad (1)$$

Here, θ is the relative phase shift between the two driving harmonics. ϕ_0 is the identical voltage amplitude of each harmonic which is fixed at 150 V in this work. The bottom electrode is grounded. The time resolved voltage drop across the plasma is measured at the top electrode by a high-voltage probe (Tektronix P6015A) connected to an oscilloscope. The amplitude of each individual harmonic and the phase shift between them are determined based on the Fourier analysis of the measured voltage waveform and are controlled by the power amplifiers and the signal generator. Figure 2 shows exemplary driving voltage waveforms for different values of

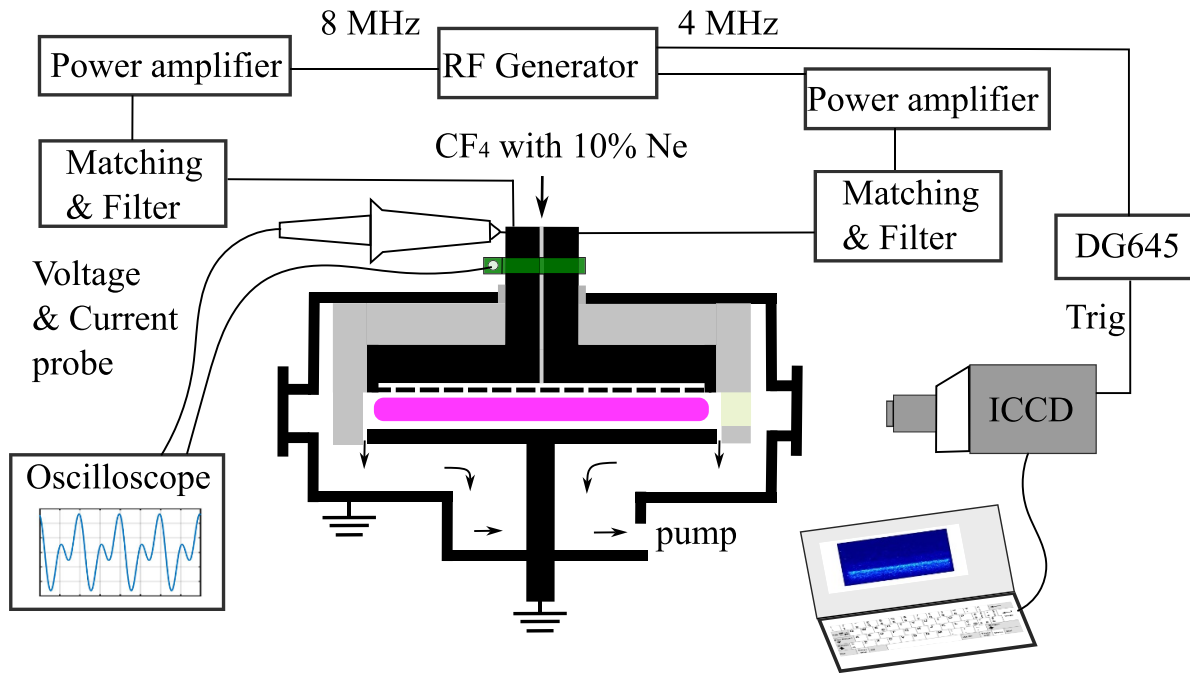


Figure 1. Sketch of the experimental setup with diagnostics.

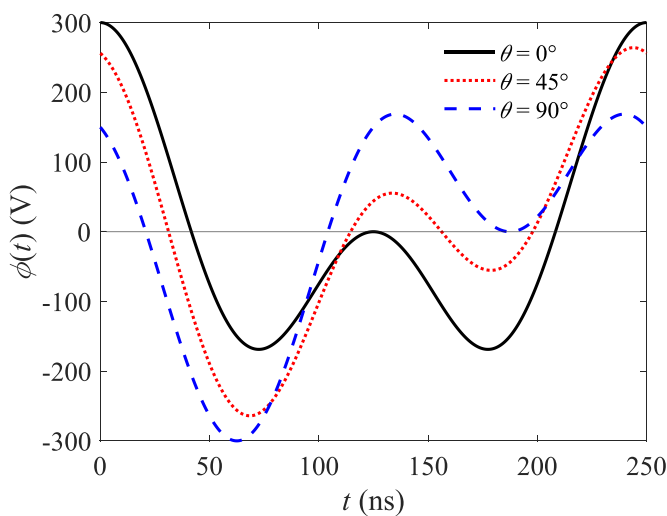


Figure 2. Driving voltage waveform as a function of time within one low frequency period for $\theta = 0^\circ, 45^\circ, 90^\circ$.

$\theta: 0^\circ, 45^\circ, \text{ and } 90^\circ$. Adjusting θ allows controlling the amplitude asymmetry of the driving voltage waveform, i.e. the difference between the absolute values of its global extrema. Due to this phase dependent electrical asymmetry a DC self-bias voltage, η , develops and can be controlled by adjusting θ in the discharge.

The discharge is operated at 100 Pa in CF_4 gas with 10% neon as a tracer gas for the PROES measurements based on a high speed intensified charged coupled device (ICCD) camera (Andor iStar DH734). The camera is triggered by a square-wave signal provided by the function generator and synchronized with the low frequency voltage waveform (4 MHz). Via

a pulse delay generator (DG645) the camera gate of 8 ns width is shifted through the fundamental RF period to realize the temporal resolution. In combination with an optical filter (center wavelength: 589 nm, full width-half maximum: 10 nm) the plasma emission resulting from a Neon emission line at 585.5 nm is measured space and time resolved within the fundamental RF period. This emission originates from the $\text{Ne}2p_1$ state, which is primarily populated by electron impact excitation from the ground state with a threshold energy of 19 eV, i.e. the spatio-temporally resolved dynamics of energetic electrons above this energy is measured. The spatial resolution of the measurements in the direction perpendicular to the electrodes is about 0.1 mm and the temporal resolution is approximately 8 ns. Based on a collisional-radiative model, the spatio-temporally resolved electron impact excitation rate from the ground state into the $\text{Ne}2p_1$ -state is determined from the measured plasma emission. More details on this model and the PROES diagnostic itself can be found elsewhere [58].

2.2. PIC/MCC simulation

To obtain access to a variety of plasma parameters, PIC/MCC simulations [59–64] are performed under conditions similar to those used in the experiments. The simulation is one-dimensional in space and three-dimensional in velocity space (1d3v). Its results are validated against experimental measurements to ensure their accuracy. In this way a correct and solid basis for analyzing the EAE in the striation mode is provided.

The simulations are performed in CF_4 , the small admixture of Ne used in the experiment is neglected, since it does not affect the plasma due to the high ionization energy of Ne compared to CF_4 [55]. The particles traced are electrons, CF_3^+ ,

Table 1. Ion-CF₄ molecule collision processes included in the simulation.

Projectile	Product	Reaction type
CF ₃ ⁺	CF ₃ ⁺	Elastic: isotropic/anisotropic
CF ₃ ⁺	CF ₃ ⁺	Reactive: keep type of ion
CF ₃ ⁺	CF ₂ ⁺	Reactive: change type of ion
CF ₃ ⁺	Minority ions	Reactive: keep type of ion as simplification
CF ₂ ⁺	CF ₂ ⁺	Elastic: isotropic/anisotropic
CF ₂ ⁺	CF ₂ ⁺	Reactive: keep type of ion
CF ₂ ⁺	Minority ions	Reactive: keep type of ion as simplification
F ⁻	F ⁻	Elastic: isotropic/anisotropic
F ⁻	F ⁻	Reactive: keep type of ion
F ⁻	e ⁻	Reactive: detachment
CF ₃ ⁻	CF ₃ ⁻	Elastic: isotropic/anisotropic
CF ₃ ⁻	CF ₃ ⁻	Reactive: keep type of ion
CF ₃ ⁻	F ⁻	Reactive: change type of ion
CF ₃ ⁻	e ⁻	Reactive: detachment

CF₂⁺, CF₃⁻, and F⁻ ions, which represent a subset of the species that exists in the plasma [60]. These species are, however, the major constituents of the plasma under the conditions of this study. The cross sections for collisions of electrons with the neutral gas are the same as those used in [65], i.e. they are originally taken from [66], with the exception of those for electron attachment processes that produce CF₃⁻ and F⁻ ions, which are adopted from [67]. In the e + CF₄ dissociative ionization collision processes producing charged species that are not included in the list of traced particles above, the loss of the electron's kinetic energy is taken into account, however, no charged particles are created.

Table 1 classifies the collisions of the various types of ions with CF₄ molecules included in the simulation according to their products. They correspond to a set of collision processes used in [68]. The treatment of ion-neutral collisions is based on the ion-molecule collision model for endothermic reactions proposed in [69], which is based on the Langevin-Hassé model and the Rice-Rampersperger-Kassel theory [70, 71]. The elastic collisions can be characterised by either isotropic and anisotropic angular scattering depending on the impact parameter of the process (see, e.g. [68]). In the other part of reactions, termed as 'reactive', a complex is formed from the incoming ion and the target CF₄ molecule, which can break up in various ways: the charged product can be (i) the same type of ion as the incoming ion (such reactions are labelled as 'reactive: keep ion type' in table 1), (ii) a type of ion that is different from the incoming ion but is included in the simulation (labelled as 'reactive: change type of ion'), (iii) an electron created in a dissociative detachment process (labelled as 'reactive: detachment'), and (iv) a type of ion that is different from the incoming ion and is not included in the simulation (labelled as 'reactive: keep type of ion as simplification'). In the latter case, the reactions produce minority ionic species, which are not considered in the code, as a simplification. Instead the original ion is kept and its tracing is continued. In this way charge conservation is ensured. We include the energy loss of the projectile

Table 2. Recombination processes considered in the simulation and the corresponding rate coefficients, where the ion and electron temperatures, T_i and T_e , are in eV.

Reaction	Rate coefficient (m ³ s ⁻¹)
CF ₃ ⁺ + e ⁻	$3.95 \times 10^{-15} T_i^{-1} T_e^{-0.5}$
CF ₃ ⁺ + F ⁻	1×10^{-13}
CF ₃ ⁺ + CF ₃ ⁻	1×10^{-13}
CF ₂ ⁺ + e ⁻	$3.95 \times 10^{-15} T_i^{-1} T_e^{-0.5}$
CF ₂ ⁺ + F ⁻	1×10^{-13}
CF ₂ ⁺ + CF ₃ ⁻	1×10^{-13}

particle due to the collision in these cases as well as in all the other types of reactive collisions.

Recombination processes between positive and negative ions as well as electrons and CF₃⁺ and CF₂⁺ are included according to the procedure of [72]. All the recombination processes and the recombination rate coefficients used in the simulation are listed in table 2. The rate coefficients for the ion-ion recombination are taken from [73], and the e⁻-CF₃⁺ from [74].

At the surfaces of the electrodes, electrons are reflected with a probability of 70%. This reflection probability was found to result in quantitatively correct simulation results for stainless steel electrodes [75]. Based on the results of a new computationally assisted diagnostic, which is introduced in section 3.1, the effective heavy particle induced SEEC is found to be $\gamma = 0.01$. Under the high pressure and low voltage conditions studied in this work, electron induced secondary electron emission can be neglected [18, 19] and, thus, is not included. The neutral gas temperature is taken to be $T_g = 350$ K. Identical to the experiment, the discharge is driven by the voltage waveform defined by equation (1) with $\phi_0 = 150$ V. The electrode gap is 1.5 cm and the neutral gas pressure is 100 Pa. The DC self-bias, η , is determined in an iterative way to ensure that the flux of the positive and negative charged particles balance at each electrode on time average [41]. The simulation results include space and time resolved values of the electron impact excitation rate of CF₄ molecules with an energy threshold of 7.54 eV and of the electron impact ionization rate of CF₄ with an energy threshold of 16 eV, which results in the production of CF₃⁺ ions [76].

3. Results

In this section, we focus on a detailed understanding of the spatio-temporally resolved electron power absorption dynamics and the quality of the separate control of the mean ion energy and flux at the electrodes as a function of the relative phase between the driving harmonics in the striation mode. To achieve good agreement between simulation and experimental results, the choice of the effective heavy particle induced SEEC in the simulation is crucially important. Therefore, in section 3.1 and based on the results of [54], we apply a new computationally assisted diagnostic to determine this surface coefficient from a comparison of the DC self-bias obtained from the simulation and the experiment. Subsequently, we then study the EAE in the striation mode in section 3.2.

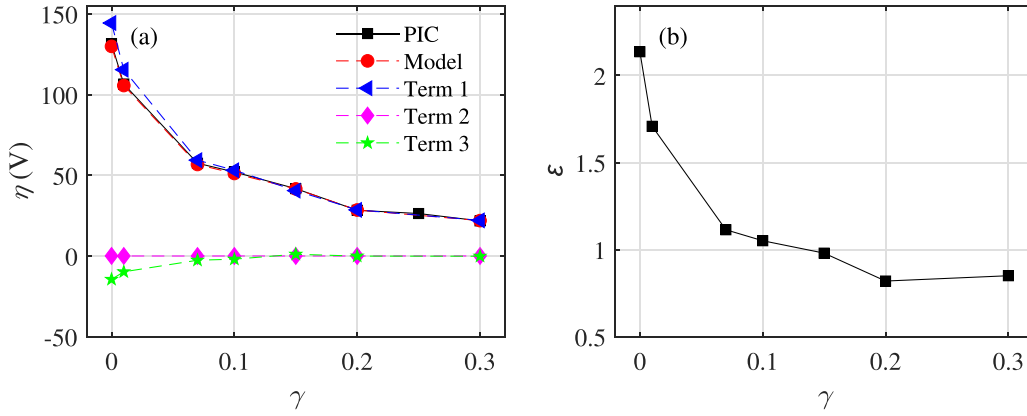


Figure 3. DC self-bias voltage, η , (a) and symmetry parameter, ϵ , (b) as a function of γ obtained from the PIC/MCC simulations and the EAE analytical model at $\theta = 105^\circ$. Discharge conditions: CF_4 , 4 MHz + 8 MHz, $\phi_0 = 150$ V, $\theta = 105^\circ$, 100 Pa, 1.5 cm electrode gap, $T_e = 350$ K, $R = 0.7$. Term 1 in (a) corresponds to the effect of the amplitude asymmetry of the applied voltage waveform on the DC self-bias, while terms 2 and 3 represent the effects of the floating potentials and the voltage drops across the bulk on the DC self-bias, respectively, according to equation (2).

3.1. Computationally assisted diagnostic to determine the effective heavy particle induced SEEC from measurements of the DC self-bias

The heavy particle induced SEEC, γ , is known to be an important input parameter in the modeling of CCPs, especially at higher pressures ($p \gtrsim 100$ Pa), at which collisional multiplication of secondary electrons inside the sheaths can play an important role. Under such conditions, γ can determine the electron power absorption mode and the plasma density, since a high value can induce a mode transition from the α - into the γ -mode. This surface coefficient is known to depend on the surface material, the incident particle species, their impact energy and angle [21, 77, 78]. For many combinations of surface materials and incident ion species it is not known well. In reactive plasmas the surface material in contact with the discharge and its characteristics are not even known accurately, since the plasma affects the surface via e.g. deposition. For these reasons surface coefficients determined from particle beam experiments based on well-defined surfaces might not describe a surface of such a material exposed to a reactive plasma well. Therefore, in-situ diagnostics for such surface coefficients that measure them under plasma exposure are important. Such diagnostics can use the dependence of distinct measurable plasma parameters on these coefficients. In combination with simulations, where such surface coefficients are input parameters and can be changed, they can be identified as those values for which a good agreement between measured and computed plasma parameters is obtained. Such computationally assisted diagnostics of γ have been developed based on PROES (γ -CAST) [55] and IEDF measurements [56] in combination with PIC/MCC simulations.

As a basis for our investigations of the EAE in CCPs operated in the striation mode, γ has to be determined realistically under the conditions used experimentally (stainless steel electrodes exposed to a CF_4 CCP at 100 Pa) to ensure accurate simulation results. To do this, a new computationally assisted diagnostic is developed, that is significantly more simple and

easier to realize in an industrial environment compared to previous methods, which require sophisticated optical or ion energy distribution measurements. It makes use of the dependence of the DC self-bias, η , on this surface coefficient, which is shown in figure 3(a) based on simulation and modeling results obtained in a CCP driven by 4 MHz and 8 MHz, $\phi_0 = 150$ V, 100 Pa and an electrode gap of 1.5 cm. Results are shown for a phase shift of $\theta = 105^\circ$, at which the DC self-bias is maximum. The electron reflection probability is set to $R = 0.7$ based on a previous study [75]. Varying R has very little effect on the DC self-bias obtained from the simulation under these discharge conditions. Measuring η is simple and typically part of any commercial CCP system. Here, it is realized by measuring the time averaged voltage drop across the plasma by a high voltage probe at the powered electrode.

Under the conditions studied in this work, there is a strong dependence of the DC self-bias on γ . Thus, a comparison of the measured DC self-bias of η obtained from the simulation for different choices of γ will yield an accurate and unique value for this surface coefficient. This strong dependence can be understood based on a model to describe the DC self-bias formation [39, 79]:

$$\eta = -\frac{\tilde{\phi}_{\max} + \epsilon \tilde{\phi}_{\min}}{1 + \epsilon} + \frac{\tilde{\phi}_{\text{sp}}^f + \epsilon \tilde{\phi}_{\text{sg}}^f}{1 + \epsilon} + \frac{\tilde{\phi}_{\max}^b + \epsilon \tilde{\phi}_{\min}^b}{1 + \epsilon}. \quad (2)$$

Here, $\tilde{\phi}_{\max}$ and $\tilde{\phi}_{\min}$ are the maximum and minimum of the applied voltage waveform, $\tilde{\phi}_{\text{sp}}^f$ and $\tilde{\phi}_{\text{sg}}^f$ are the floating potentials at the powered and grounded electrodes, which correspond to the minimum voltage drops across the respective sheath within each period of the fundamental driving frequency. $\tilde{\phi}_{\max}^b$ and $\tilde{\phi}_{\min}^b$ are the voltage drops across the plasma bulk at the times of maximum and minimum applied voltage, respectively. ϵ is the symmetry parameter:

$$\epsilon = \left| \frac{\hat{\phi}_{\text{sg}}}{\hat{\phi}_{\text{sp}}} \right| = \left(\frac{A_p}{A_g} \right)^2 \frac{\bar{n}_{\text{sp}}}{\bar{n}_{\text{sg}}} \left(\frac{Q_{\text{mg}}}{Q_{\text{mp}}} \right)^2 \frac{I_{\text{sg}}}{I_{\text{sp}}} \approx \frac{\bar{n}_{\text{sp}}}{\bar{n}_{\text{sg}}} \left(\frac{Q_{\text{mg}}}{Q_{\text{mp}}} \right)^2, \quad (3)$$

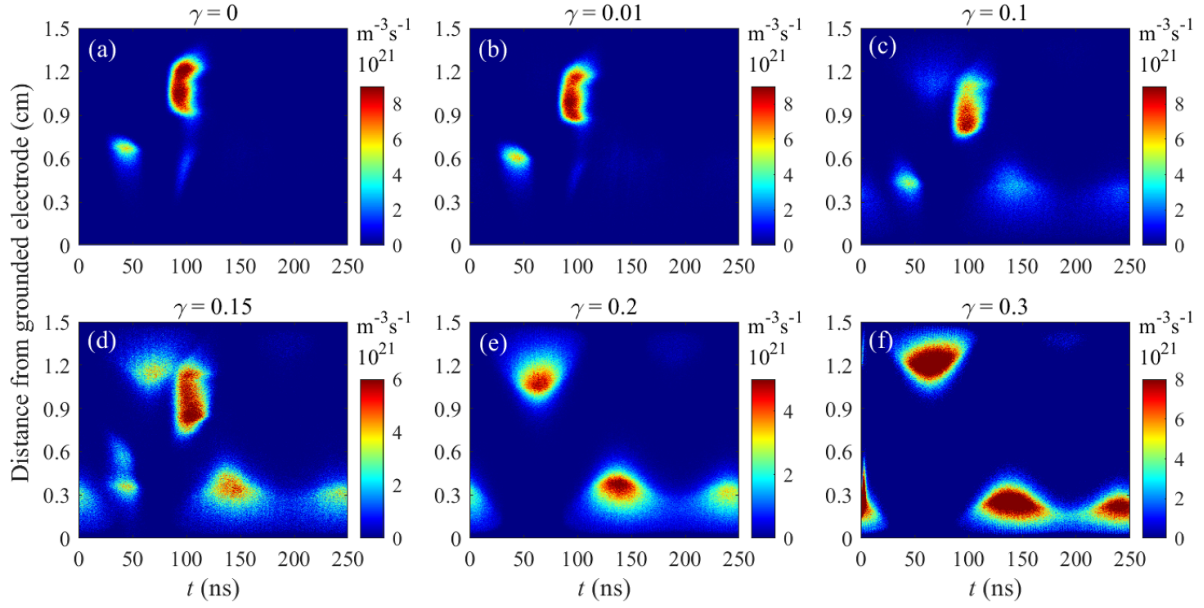


Figure 4. Spatio-temporal distribution of the ionization rate for different values of γ obtained from the PIC/MCC simulations at $\theta = 105^\circ$. Discharge conditions: CF_4 , 4 MHz + 8 MHz, $\theta = 105^\circ$, $\phi_0 = 150$ V, 100 Pa, 1.5 cm electrode gap, $T_g = 350$ K, $R = 0.7$. The results are obtained by averaging over 1000 low frequency cycles.

where $|\hat{\phi}_{\text{sp}}|$ and $|\hat{\phi}_{\text{sg}}|$ are the maximum voltage drops across the sheath at the powered and grounded electrode. A_p, A_g are the surface areas of the powered and grounded electrode, $Q_{\text{mp/g}}$ are the maximum uncompensated charges in each sheath. $\bar{n}_{\text{sp/sg}}$, are the spatially and temporally averaged ion densities in the respective sheath. $I_{\text{sp}}, I_{\text{sg}}$ are the sheath integrals for the powered and grounded electrode sheath, respectively [79]. In this work, $A_p = A_g$, and $I_{\text{sp}}/I_{\text{sg}} \approx 1$ [39]. All the remaining input parameters of the model are taken from the PIC/MCC simulation in this work, while the sheath widths are defined according to the Brinkmann sheath model [80].

The DC self-bias obtained from this model as well as the contributions of each of the three terms of equation (2) and the symmetry parameter are shown as a function of γ in figures 3(a) and (b), respectively. Excellent agreement with the DC self-bias obtained directly from the simulation is found. This shows that the model yields realistic results. The first term of equation (2) provides the dominant contribution. The third term yields a minor contribution at low values of γ , for which the plasma density and conductivity are low and a significant voltage drops across the plasma bulk. At higher values of γ the third term is negligible. The dependence of η on γ is strongly linked to the change of the symmetry parameter $\varepsilon \approx \bar{n}_{\text{sp}}/\bar{n}_{\text{sg}}$ with the heavy particle induced SEEC shown in figure 3(b). This trend is explained by the effects of γ on the spatio-temporally resolved ionization dynamics shown in figure 4. At low values of γ and for a phase shift of 105° , a weak maximum of the ionization rate is observed at $t \approx 50$ ns. At this time within the low frequency period, when the sheath at the top electrode expands, and as discussed in detail in [50], electrons are accelerated downwards (i.e. towards the grounded electrode) by a strong bulk electric field that is caused by the high instantaneous conduction current in combination with

a low bulk conductivity due to the high electronegativity of the plasma. In this way the mean electron energy is increased and ionization occurs close to the instantaneous sheath edge at the bottom electrode. Due to the shape of the driving voltage waveform at this phase shift, the conduction current flows in the opposite direction shortly after this time at approximately $t \approx 90$ ns. This leads to an acceleration of electrons towards the top electrode and a much stronger ionization maximum in its vicinity at this time. This ionization maximum at the top electrode is stronger than the one observed at the bottom electrode earlier, because warm electrons, heated at $t \approx 50$ ns are accelerated upwards at $t \approx 90$ ns and their energy is further increased, when the current reverses its direction, so that more ionization happens, but now close to the top electrode. Thus, for low values of γ the mean ion density in the sheath at the top electrode is higher than the density in the bottom sheath and the symmetry parameter is larger than unity. Combined with the amplitude asymmetry of the driving voltage waveform at 105° ($|\hat{\phi}_{\text{max}}| < |\hat{\phi}_{\text{min}}|$), this yields a strong positive DC self-bias. As shown in figure 4, increasing γ results in a mode transition into the γ -mode, where ionization by secondary electron avalanches inside the sheaths at the times of high local sheath voltage dominates. Due to the particular shape of the driving voltage waveform at $\theta = 105^\circ$, the sheath at the bottom grounded electrode is expanded for a longer time compared to the sheath at the top electrode. Therefore, in the γ -mode more ionization occurs close to the bottom electrode so that the local ion density is higher compared to the one at the top electrode and the symmetry is reversed, i.e. $\varepsilon < 1$.

Figure 5 shows the axial profiles of the time-averaged charged species densities for different values of γ . For $\gamma < 0.2$, the discharge is strongly electronegative with the dominance of CF_3^+ and F^- ions in the bulk region and the formation of

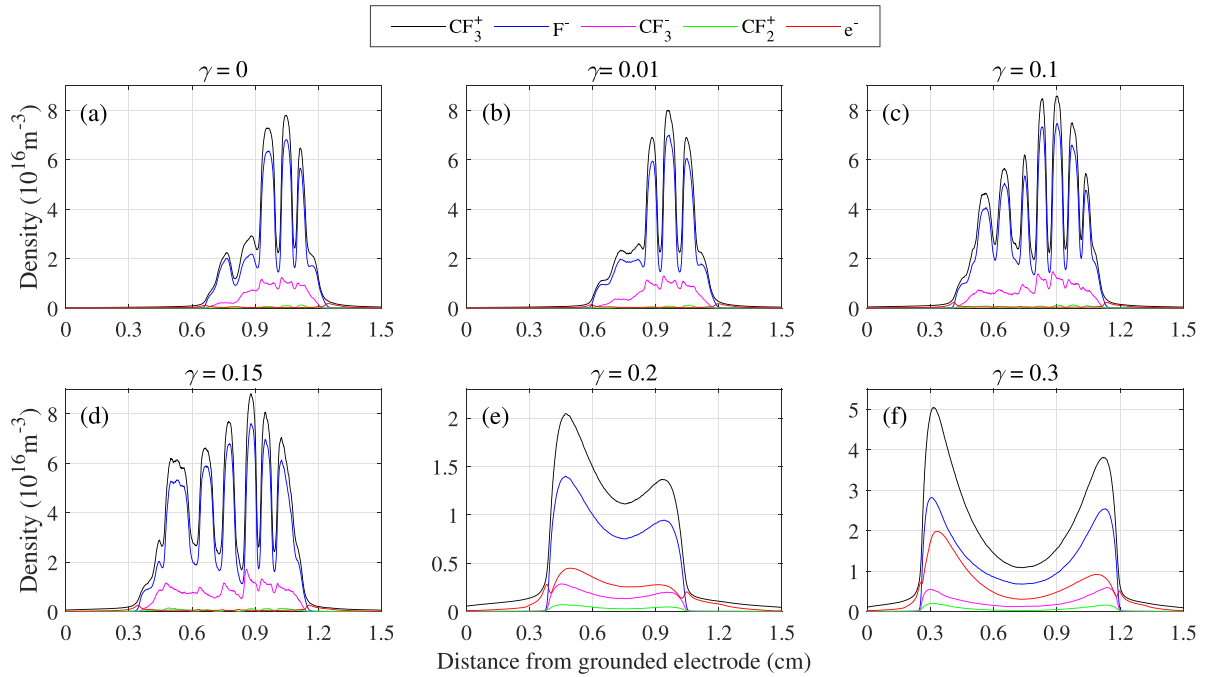


Figure 5. Time averaged charged particle density profiles for different values of γ obtained from the PIC/MCC simulations at $\theta = 105^\circ$. Discharge conditions: CF_4 , 4 MHz + 8 MHz, $\theta = 105^\circ$, $\phi_0 = 150$ V, 100 Pa, 1.5 cm electrode gap, $T_g = 350$ K, $R = 0.7$. The results are obtained by averaging over 1000 low frequency cycles.

striations is observed. As $\varepsilon > 1$, the maximum sheath voltage at the grounded electrode is larger compared to the one at the powered electrode and, thus, the maximum sheath width is larger at the grounded electrode so that the bulk region including the striations is shifted towards the powered electrode. Increasing γ induces a transition into the γ -mode, makes the plasma more electropositive and results in the disappearance of the striations.

Based on the comparison between computational and experimental results for the DC self-bias, $\gamma = 0.01$ is found to yield the best match for the conditions investigated in this work. Figure 6 shows a comparison of the computationally obtained DC self-bias, based on $\gamma = 0.01$, and the measured data as a function of θ . The computational results are illustrated by vertical bars, whose height corresponds to the fluctuation of the DC self-bias at the respective phase caused by a plasma instability. This instability is believed to be a real physical phenomenon and will be described in more detail in the following section. Excellent agreement between experimental and computational data is found. Based on these results, we conclude that $\gamma = 0.01$ is the correct value of the effective heavy particle induced SEEC under the conditions studied in this work. This value will be used in section 3.2, where the EAE in the striation mode is investigated based on computational and experimental results. According to Phelps and Petrovic [77], such a low value of γ is realistic for dirty surfaces at the low mean ion energies of 20 to 40 eV observed in this work (see figure 10). It also agrees approximately with the value obtained from the empirical formula $\gamma = 0.016 \cdot (E_i - 2E_w)$, that allows to

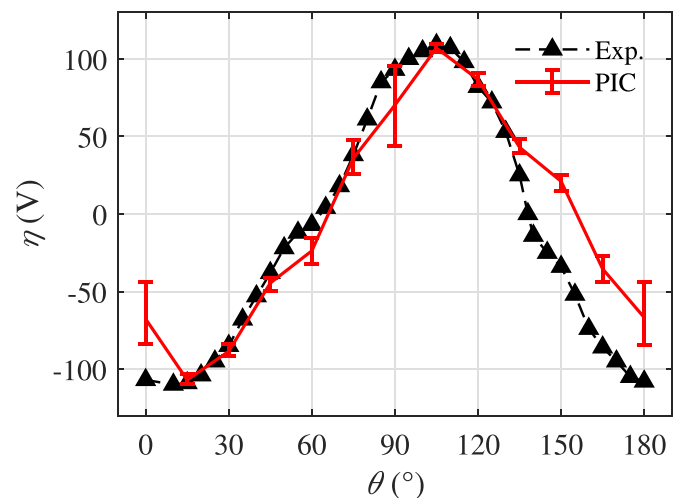


Figure 6. Measured and computationally obtained DC self-bias, η , as a function of θ . The computational results are illustrated by vertical bars, whose height corresponds to the fluctuation of the DC self-bias at the respective phase caused by a plasma instability. Discharge conditions: CF_4 , 4 MHz + 8 MHz, $\phi_0 = 150$ V, $\theta = 105^\circ$, 100 Pa, 1.5 cm electrode gap. In the simulation, $T_g = 350$ K, $R = 0.7$, and $\gamma = 0.01$ are used.

estimate this surface coefficient in the presence of Auger emission of secondary electrons [81]. Using the ionization potential of CF_3 of $E_i \approx 8.8$ eV and the work function of stainless steel of $E_w \approx 4.1$ eV yields $\gamma \approx 0.01$ in agreement with our results.

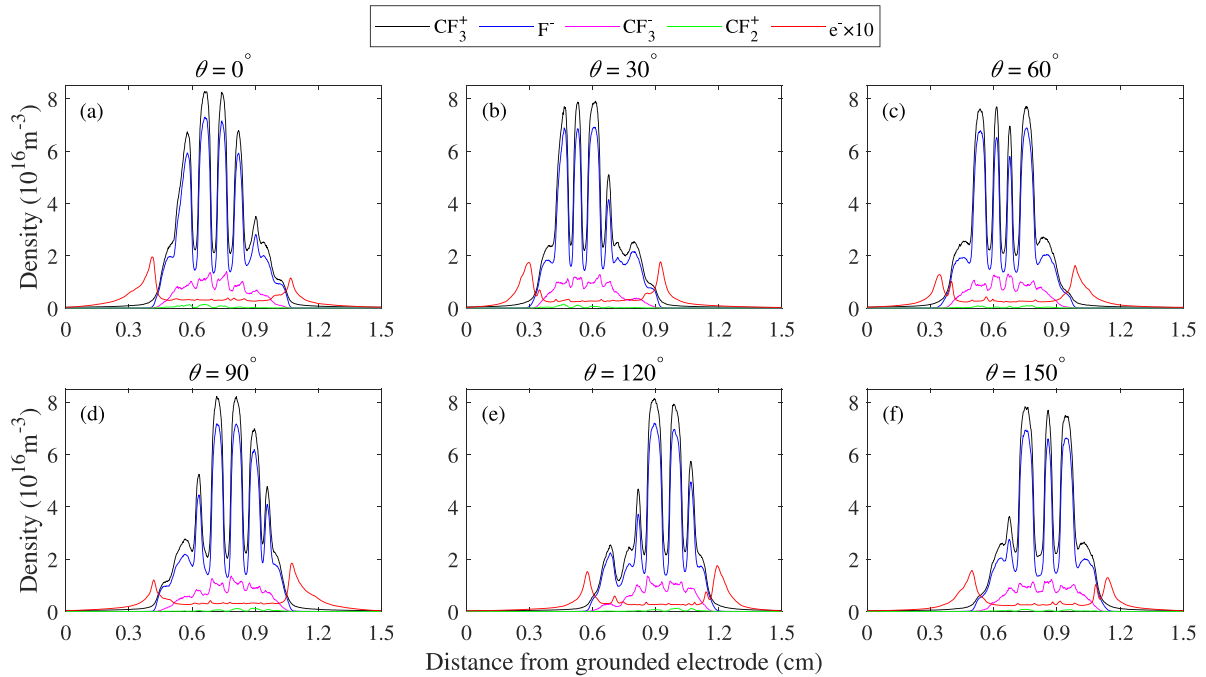


Figure 7. Charged particle density profiles obtained from the simulation and averaged over 50 low frequency cycles as a function of θ . Discharge conditions: CF_4 , 4 MHz + 8 MHz, $\phi_0 = 150$ V, 100 Pa, 1.5 cm electrode gap, $T_g = 350$ K, $R = 0.7$ and $\gamma = 0.01$.

3.2. The electrical asymmetry effect in the striation mode

In this section, the EAE and the quality of the separate control of the mean ion energy and flux at the electrodes via phase control are investigated in CF_4 discharges operated in the striation mode (at 100 Pa, $f = 4$ MHz, and $\phi_0 = 150$ V) based on experimental and simulation results. In the simulation, an electron reflection probability of $R = 0.7$ and an effective heavy particle induced SEEC of $\gamma = 0.01$ (based on the results of section 3.1) are used to describe the stainless steel electrodes exposed to a CF_4 discharge in the experiment.

Figure 7 shows the charged particle densities profiles obtained from the simulation and time averaged over 50 consecutive low frequency period for different values of θ . The formation of ‘comb-like’ density profiles is observed at all phases, i.e. the discharge is operated in the striation mode. The dominant positively and negatively charged particle species are CF_3^+ and F^- ions, i.e. the discharge is strongly electronegative, since the electron density is much lower than the negative ion density in the plasma bulk. The densities of CF_3^+ and F^- are also much higher than those of CF_2^+ and CF_3^- ions. The negative ions are confined to the electronegative bulk region, while electropositive edge regions form in front of each electrode and close to the position of maximum sheath width. In such regions, a local maximum of the electron density is observed similar to previous studies of electronegative plasmas [65, 69, 82, 83]. Changing the phase, θ , leads to an axial shift of the striation pattern, a change of the number of pronounced striations, and also affects the ratio of the electron density maxima located close to the electrodes in the electropositive edge regions of the plasma.

Averaging the simulation data over a higher number of consecutive low frequency periods results in smeared-out striation

patterns as illustrated in figure 8, that shows charged particle density profiles obtained from the simulation after averaging over 1000 consecutive low frequency periods. This effect is the result of a plasma instability observed in the simulation as an oscillation of plasma parameters on the millisecond-timescale, which includes periodic fluctuations of the DC self-bias as indicated in figure 6. The effect of this instability on the time averaged charged particle density profiles and the DC self-bias is phase-dependent. At 60° and 150° its effect on the charged particle density profiles, i.e. the extent to which the striations are smeared-out, is less pronounced as compared to 0° , 30° , 90° , and 120° . This is caused by a phase-dependent periodic movement of the striations as a consequence of the instability. Such instabilities are known to occur in electronegative CCPs and were observed before experimentally [84, 85]. They can be caused by attachment induced periodic changes of the mean electron energy. While the physics of this instability is not a topic of this work, but will be investigated separately in the future, it is important to point out that it exists and affects plasma parameters obtained by diagnostics that are based on temporal averaging over long periods of time such as PROES. Our simulation results show that less pronounced striated patterns will be observed by such diagnostics, although the striations are actually more pronounced, but their positions depend on time, i.e. they are not entirely stationary.

The effects of the phase, θ , on the charged particle density profiles can be understood based on the spatio-temporally resolved excitation and ionization dynamics. Experimentally and computationally obtained results are shown in figure 9. The white lines in the last two rows of figure 9 indicate the positions of the sheath edges according to the Brinkmann sheath model [80]. To compare the simulation results with the PROES

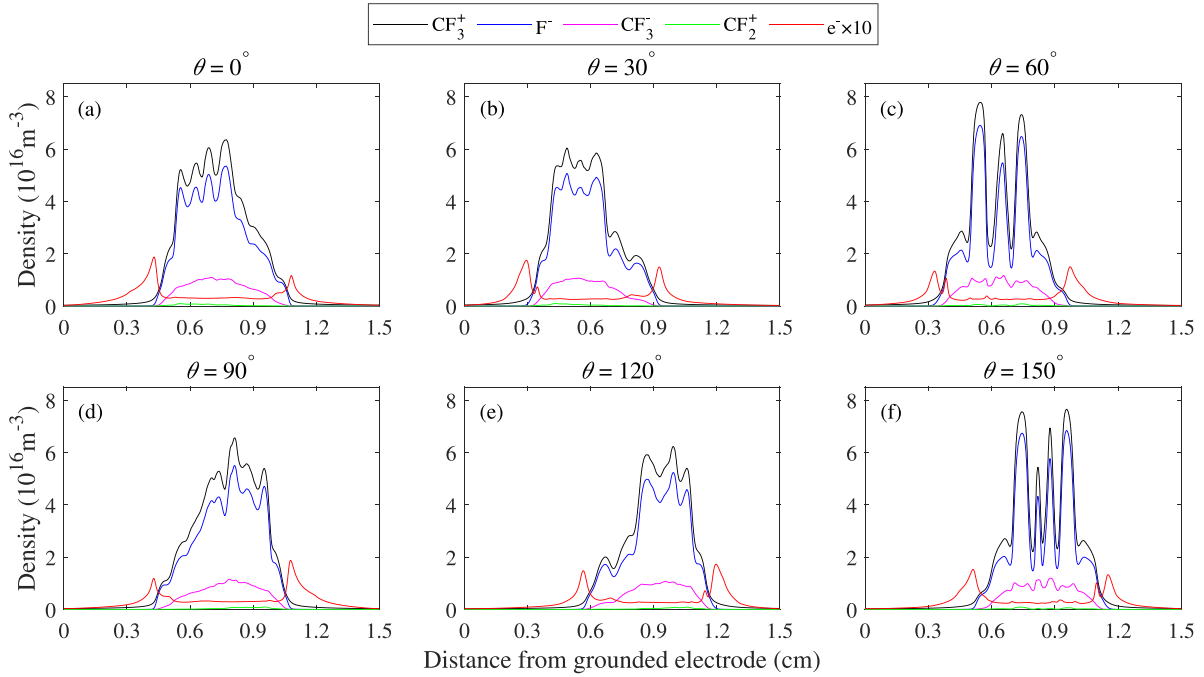


Figure 8. Charged particle density profiles obtained from the simulation and averaged over 1000 low frequency cycles as a function of θ . Discharge conditions: CF_4 , 4 MHz + 8 MHz, $\phi_0 = 150$ V, 100 Pa, 1.5 cm electrode gap, $T_g = 350$ K, $R = 0.7$ and $\gamma = 0.01$.

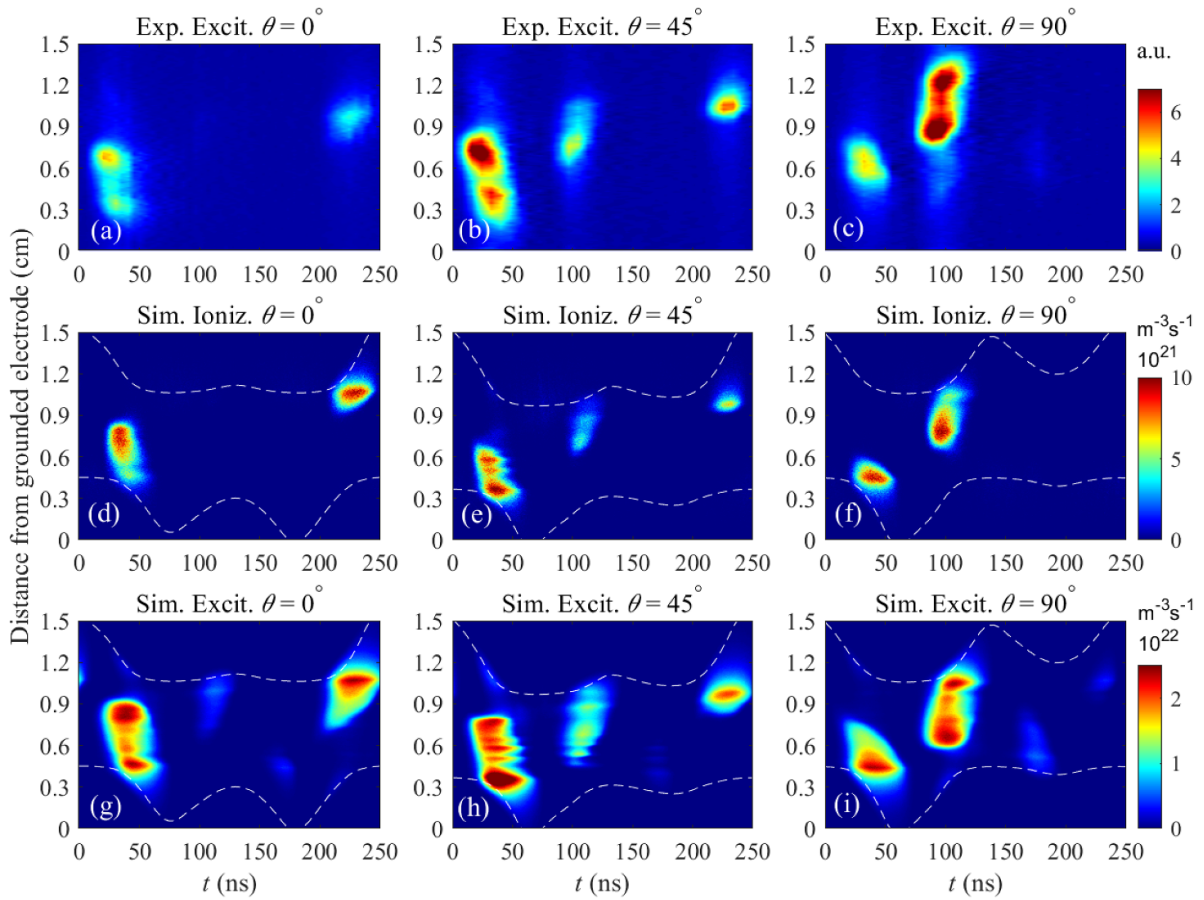


Figure 9. Spatio-temporal distributions of the measured electron impact excitation rate from the ground state into $\text{Ne}2p_1$ obtained by PROES (first row), computationally obtained ionization rate (second row) and electron impact excitation rate of CF_4 (third row). Results are shown for $\theta = 0^\circ$ (first column), 45° (second column) and 90° (third column). The computational data are obtained based on averaging the simulation results over 1000 low frequency cycles. Discharge conditions: CF_4 (+ 10% Ne admixture in the experiment), 4 MHz + 8 MHz, $\phi_0 = 150$ V, 100 Pa, 1.5 cm electrode gap. In the simulation, $T_g = 350$ K, $R = 0.7$, and $\gamma = 0.01$ are used.

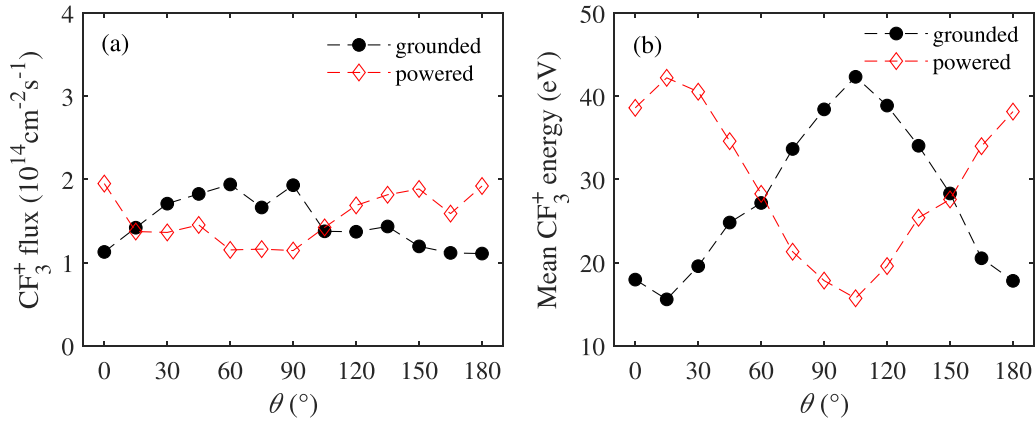


Figure 10. CF_3^+ ion flux and mean ion energy at both electrodes as a function of θ resulting from the PIC simulation. Discharge conditions: CF_4 , 4 MHz + 8 MHz, $\phi_0 = 150$ V, 100 Pa, 1.5 cm electrode gap, $T_g = 350$ K, $R = 0.7$ and $\gamma = 0.01$.

measurements, the computationally obtained data are averaged over 1000 low frequency periods. Excellent agreement between experimental and simulation results is found for all phase angles. Small differences might be explained by the different electron energy thresholds for the different processes and the 10% Ne admixture in the experiment. Due to the limited spatial resolution of the PROES diagnostic in the experiment the small gap in between adjacent striations cannot be resolved as sharply as in the simulation. In agreement with the results for the charged particle density profiles shown in figure 8 and due to the observed plasma instability in combination with the temporal averaging of the results, more pronounced striations are observed at 45° compared to 0° and 90° . For 90° phase, a high electron current flows from the top (powered) to the bottom (grounded) electrode at $t \approx 50$ ns and in the reversed direction at $t \approx 100$ ns. Correspondingly cold electrons are accelerated downwards at the first half period of the high frequency and shortly later, at the next half period, warm electrons (heated by the earlier acceleration), are accelerated upwards. Therefore, more ionization occurs close to the top electrode at this phase and the electron density maximum is higher on this side compared to the bottom electrode (see figure 8(d)). The reversed effect occurs at $\theta = 0^\circ$ so that the electron density is higher at the bottom electrode at this phase (see figure 8(a)). In accordance with the change of the DC self-bias and the spatio-temporal ionization dynamics, the striations are shifted axially by changing θ . They are shifted towards the electrode, where more ionization happens for the respective phase. During plasma breakdown, the striations will form at positions where the local ion plasma frequencies are high enough to allow the ions to follow the bulk electric field. This requires high local plasma densities and, thus, the formation of striations is more pronounced close to the electrode, where more ions are generated. For $\theta = 45^\circ$, the electron current that flows in the plasma bulk from the top to the bottom electrode at $t \approx 50$ ns is stronger than the reversed electron current maxima at $t \approx 100$ ns and $t \approx 230$ ns. Thus, there is strong ionization at the bottom electrode.

Figure 10 shows the ion flux and the mean energy of CF_3^+ ions at the powered (red line) and grounded (black line)

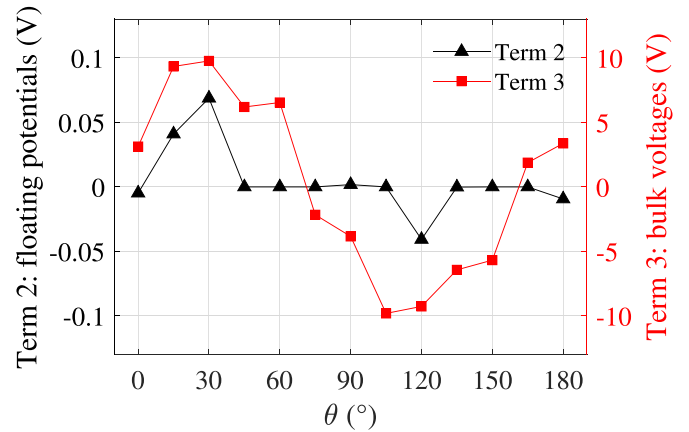


Figure 11. Second and third terms of equation (2) as a function of θ , which correspond to the contributions of the floating potentials and the bulk voltage drops to the DC self-bias, respectively. Discharge conditions: CF_4 , 4 MHz + 8 MHz, $\phi_0 = 150$ V, 100 Pa, 1.5 cm electrode gap, $T_g = 350$ K, $R = 0.7$ and $\gamma = 0.01$.

electrode as a function of θ . As a consequence of the phase control of the DC self-bias, figure 10(b) shows that the mean ion energy can be tuned via the EAE. The mean ion energy can be adjusted between 15 eV and 42 eV based on the phase control of the DC self-bias, η , shown in figure 6. Previous studies of CF_4 discharges [50] demonstrated that the electrical control range of the DC self-bias is reduced in electronegative compared to electropositive CCP to only about 22% of the peak-to-peak value of the driving voltage because of the high bulk voltage drop. The same is true under the discharge conditions studied in this work. Figure 11 shows that the bulk voltage drop indeed leads to a positive contribution to the DC self-bias for $\theta \leq 60^\circ$. As the total DC self-bias is negative for a phase within this range (see figure 6), the strong electronegativity of the plasma and the related voltage drop across the bulk reduce the electrical control range of η and of the mean ion energy as compared to electropositive CCPs. The same occurs at larger phase shifts, at which η is positive, but the bulk voltage drop yields a negative contribution to the DC self-bias. In this work,

the phase control allows to tune η within a range that corresponds to about 21% of the peak-to-peak value of the driving voltage waveform. This is less than the control range typically accessible in electropositive CCPs [42], so that the separate control of ion properties is more limited in electronegative compared to electropositive CCPs, but it is similar to the range accessible in electronegative CCPs operated in CF_4 in the absence of striations [50]. As shown in figure 10(a), the ion flux at both electrodes remains approximately constant. It changes by less than 30% with respect to its averaged value of the phase at both electrodes. The small changes of the ion flux are caused by the phase dependence of the ionization rate at each electrode as a consequence of the bulk electron heating, which is similar compared to previous findings in electronegative discharges in the absence of striations [50]. Overall, the quality of the separate control of these ion characteristics via the EAE in the presence of striations is good and, under the discharge conditions studied here, is not reduced compared to electronegative CCPs operated in the DA-mode in the absence of striations.

4. Conclusions

The electron power absorption dynamics and the quality of the separate control of the mean ion energy and flux at the electrodes of a CCP operated in CF_4 in the striation mode under the conditions of the EAE were investigated based on PIC/MCC simulations, modelling and experiments. To ensure the presence of striations, the plasma was operated at 100 Pa pressure. The EAE was established by the superposition of 4 MHz and 8 MHz sinusoidal voltage waveforms with adjustable relative phase to excite the discharge.

The simulation results were validated against experimental PROES measurements of the spatio-temporally resolved excitation dynamics of energetic electrons and measurements of the DC self-bias as a function of the phase. The simulations indicated that the DC self-bias, η , exhibits a strong dependence on the heavy particle induced SEEC, γ , used as an input parameter in the simulation. This behavior allowed us to determine the actual value of the effective γ coefficient in the experiment by comparing the experimentally measured DC self-bias value with the computational results obtained via scanning the value of this coefficient. As this diagnostic method is only based on a non-intrusive measurement of the DC self-bias, which is typically part of any CCP system, it can be applied easily. For the stainless steel electrodes exposed to a CF_4 plasma under the conditions studied, a value of $\gamma = 0.01$ was found. Based on this SEEC, excellent agreement between simulation and experimental results for (i) the dependence of the DC self-bias voltage on the phase difference between the RF excitation harmonics and (ii) the dynamics of the fast electrons (manifesting in the spatio-temporal distributions of the excitation rates) was obtained.

An oscillating plasma instability on the millisecond timescale was observed in the simulations. The presence of this

instability was demonstrated to lead to fluctuations of the DC self-bias and to smearing-out the axial striation patterns.

A detailed analysis of the spatio-temporal electron power absorption dynamics was performed. Strong bulk heating of electrons at the times of high RF current within each low frequency period was observed due to a high bulk electric field caused by a depleted conductivity as a result of the high electronegativity. The spatial distributions of the ionization and excitation rates, that result from electrons accelerated by this electric field, were found to be affected by the presence of the striations, that locally change the bulk electric field. The electron heating, excitation and ionization dynamics were found to depend on the relative phase between the driving harmonics in a way that results only in a weak dependence of the positive ion flux at each electrode as a function of θ , while the mean ion energy can be tuned over a wide range via phase control due to the change of the DC self-bias via the EAE. Tuning the phase was also found to result in an axial shift of the striation patterns and in a change of the number of striations. However, no detrimental effects of the presence of striations on the separate control of these process relevant ion characteristics were found as compared to CCPs operated in electronegative gases in the absence of striations.

These results are expected to be relevant for knowledge based plasma process development and control in commercial CCPs, which are often operated in electronegative and reactive gases. They demonstrate that the EAE is an attractive option to realize such control even under such conditions and in complex modes of discharge operation such as the striation-mode.

Data availability statement

All data that support the findings of this study are included within the article (and any supplementary files).

Acknowledgments


This work has been financially supported by the National Natural Science Foundation of China (NSFC) (Grants Nos. 12275043, 11935005 and 1202101005), the Fundamental Research Funds for the Central Universities (No. DUT21TD104), China Scholarship Council (No. 202106060085) and the Hungarian National Office for Research, Development, and Innovation (NKFIH) via the Grant K134462. We would like to extend our sincere thanks to Mate Vass for his support on analyzing the electron dynamics.

ORCID iDs

Xiao-Kun Wang  <https://orcid.org/0000-0003-4160-5316>

Ranna Masheyeva  <https://orcid.org/0000-0002-6950-662X>

Yong-Xin Liu  <https://orcid.org/0000-0002-6506-7148>

Julian Schulze  <https://orcid.org/0000-0001-7929-5734>

Zoltán Donkó  <https://orcid.org/0000-0003-1369-6150>

References

- [1] Lieberman M A and Lichtenberg A J 2005 *Principles of Plasma Discharges and Materials Processing* 2nd edn (Wiley Interscience)
- [2] Makabe T and Petrovic Z L 2006 *Plasma Electronics: Applications in Microelectronic Device Fabrication* (CRC Press)
- [3] Donnelly V M and Kornblit A 2013 *J. Vac. Sci. Technol. A* **31** 050825
- [4] Balachova O, Alves M, Swart J, Braga E and Cescato L 2000 *Microelectron. J.* **31** 213–5
- [5] Takagi S, Onoue S, Nishitani K, Shinnmura T and Shigesato Y 2015 *Japan. J. Appl. Phys.* **54** 036501
- [6] d'Agostino R and Flamm D L 1981 *J. Appl. Phys.* **52** 162–7
- [7] Makabe T 2022 *J. Phys. D: Appl. Phys.* **56** 045203
- [8] Yang S, Lin H, Zhang T, Peng Y and Zhang Q 2022 *Plasma Sources Sci. Technol.* **31** 125007
- [9] Wu H, Chen Z, Wang Z, Rao B, Jiang W and Zhang Y 2022 *J. Phys. D: Appl. Phys.* **55** 255203
- [10] Belenguer P and Boeuf J P 1990 *Phys. Rev. A* **41** 4447
- [11] Schulze J, Heil B G, Luggenholscher D and Czarnetzki U 2008 *IEEE Trans. Plasma Sci.* **36** 1400–1
- [12] Schulze J, Donkó Z, Lafleur T, Wilczek S and Brinkmann R P 2018 *Plasma Sources Sci. Technol.* **27** 055010
- [13] Turner M M 1995 *Phys. Rev. Lett.* **75** 1312
- [14] Lafleur T, Chabert P and Booth J P 2014 *Plasma Sources Sci. Technol.* **23** 035010
- [15] Mussenbrock T and Brinkmann R P 2006 *Appl. Phys. Lett.* **88** 151503
- [16] Bora B, Bhuyan H, Favre M, Wyndham E and Chuaqui H 2012 *Appl. Phys. Lett.* **100** 094103
- [17] Schuengel E, Brandt S, Donkó Z, Korolov I, Derzsi A and Schulze J 2015 *Plasma Sources Sci. Technol.* **24** 044009
- [18] Horváth B, Daksha M, Korolov I, Derzsi A and Schulze J 2017 *Plasma Sources Sci. Technol.* **26** 124001
- [19] Horváth B, Schulze J, Donkó Z and Derzsi A 2018 *J. Phys. D: Appl. Phys.* **51** 355204
- [20] Schulze J, Donkó Z, Schüngel E and Czarnetzki U 2011 *Plasma Sources Sci. Technol.* **20** 045007
- [21] Daksha M, Derzsi A, Mujahid Z, Schulenberg D, Berger B, Donkó Z and Schulze J 2019 *Plasma Sources Sci. Technol.* **28** 034002
- [22] Schulze J, Derzsi A, Dittmann K, Hemke T, Meichsner J and Donkó Z 2011 *Phys. Rev. Lett.* **107** 275001
- [23] Liu G H, Liu Y X, Wen D Q and Wang Y N 2015 *Plasma Sources Sci. Technol.* **24** 034006
- [24] Liu Y X, Schüngel E, Korolov I, Donkó Z, Wang Y N and Schulze J 2016 *Phys. Rev. Lett.* **116** 255002
- [25] Liu Y X, Korolov I, Schüngel E, Wang Y N, Donkó Z and Schulze J 2017 *Plasma Sources Sci. Technol.* **26** 055024
- [26] Liu Y X, Korolov I, Schüngel E, Wang Y N, Donkó Z and Schulze J 2017 *Phys. Plasmas* **24** 073512
- [27] Liu Y X, Donkó Z, Korolov I, Schüngel E, Wang Y N and Schulze J 2019 *Plasma Sources Sci. Technol.* **28** 075005
- [28] Wang X K, Wang X Y, Liu Y X, Schulze J, Donkó Z and Wang Y N 2022 *Plasma Sources Sci. Technol.* **31** 064002
- [29] Wang L, Wen D Q, Zhang Q Z, Song Y H, Zhang Y R and Wang Y N 2019 *Plasma Sources Sci. Technol.* **28** 055007
- [30] Georgieva V and Bogaerts A 2005 *J. Appl. Phys.* **98** 023308
- [31] Gans T, Schulze J, O'Connell D, Czarnetzki U, Faulkner R, Ellingboe A R and Turner M M 2006 *Appl. Phys. Lett.* **89** 261502
- [32] Turner M M and Chabert P 2006 *Phys. Rev. Lett.* **96** 205001
- [33] Kawamura E, Lieberman M A and Lichtenberg A J 2006 *Phys. Plasmas* **13** 053506
- [34] Wang S B and Wendt A E 2000 *J. Appl. Phys.* **88** 643
- [35] Patterson M M, Chu H Y and Wendt A E 2007 *Plasma Sources Sci. Technol.* **16** 257
- [36] Schulze J, Schüngel E, Donkó Z and Czarnetzki U 2011 *Plasma Sources Sci. Technol.* **20** 015017
- [37] Lafleur T 2016 *Plasma Sources Sci. Technol.* **25** 013001
- [38] Heil B G, Schulze J, Mussenbrock T, Brinkmann R P and Czarnetzki U 2008 *IEEE Trans. Plasma Sci.* **36** 1404
- [39] Heil B G, Czarnetzki U, Brinkmann R P and Mussenbrock T 2008 *J. Phys. D: Appl. Phys.* **41** 165202
- [40] Czarnetzki U, Heil B G, Schulze J, Donkó Z, Mussenbrock T and Brinkmann R P 2009 *J. Phys.: Conf. Ser.* **162** 012010
- [41] Donkó Z, Schulze J, Heil B G and Czarnetzki U 2008 *J. Phys. D: Appl. Phys.* **42** 025205
- [42] Schulze J, Schüngel E and Czarnetzki U 2009 *J. Phys. D: Appl. Phys.* **42** 092005
- [43] Schulze J, Schüngel E, Donkó Z and Czarnetzki U 2010 *Plasma Sources Sci. Technol.* **19** 045028
- [44] Korolov I, Donkó Z, Czarnetzki U and Schulze J 2012 *J. Phys. D: Appl. Phys.* **45** 465205
- [45] Schüngel E, Zhang Q Z, Iwashita S, Schulze J, Hou L J, Wang Y N and Czarnetzki U 2011 *J. Phys. D: Appl. Phys.* **44** 285205
- [46] Schüngel E, Eremin D, Schulze J, Mussenbrock T and Czarnetzki U 2012 *J. Appl. Phys.* **112** 053302
- [47] Zhang Q Z, Jiang W, Hou L J and Wang Y N 2011 *J. Appl. Phys.* **109** 013308
- [48] Lafleur T, Chabert P and Booth J P 2013 *J. Phys. D: Appl. Phys.* **46** 135201
- [49] Korolov I, Derzsi A, Donkó Z and Schulze J 2013 *Appl. Phys. Lett.* **103** 064102
- [50] Schulze J, Derzsi A and Donkó Z 2011 *Plasma Sources Sci. Technol.* **20** 045008
- [51] Fischer G, Ouaras K, Drahi E, Bruneau B and Johnson E V 2018 *Plasma Sources Sci. Technol.* **27** 074003
- [52] Bruneau B et al 2016 *J. Appl. Phys.* **119** 163301
- [53] Skarphedinsson G A and Gudmundsson J T 2020 *Plasma Sources Sci. Technol.* **29** 084004
- [54] Masheyeva R U, Dzhumagulova K N, Myrzaly M, Schulze J and Donkó Z 2021 *AIP Adv.* **11** 075024
- [55] Daksha M, Berger B, Schuengel E, Korolov I, Derzsi A, Koepke M, Donkó Z and Schulze J 2016 *J. Phys. D: Appl. Phys.* **49** 234001
- [56] Schulze C, Donkó Z and Benedikt J 2022 *Plasma Sources Sci. Technol.* **31** 105017
- [57] Franek J, Brandt S, Berger B, Liese M, Barthel M, Schüngel E and Schulze J 2015 *Rev. Sci. Instrum.* **86** 053504
- [58] Schulze J, Schüngel E, Donkó Z, Luggenholscher D and Czarnetzki U 2010 *J. Phys. D: Appl. Phys.* **43** 124016
- [59] Denpoh K 2020 *Japan. J. Appl. Phys.* **60** 016002
- [60] Denpoh K and Nanbu K 2022 *J. Vac. Sci. Technol.* **40** 063007
- [61] Sun A, Becker M M and Loffhagen D 2018 *Plasma Sources Sci. Technol.* **27** 054002
- [62] Gudmundsson J T, Krek J, Wen D Q, Kawamura E and Lieberman M A 2022 *Plasma Sources Sci. Technol.* **30** 125011
- [63] Wen D Q, Krek J, Gudmundsson J T, Kawamura E, Lieberman M A and Verboncoeur J P 2022 *IEEE Trans. Plasma Sci.* **50** 2548–57
- [64] Yang D, Wang H, Zheng B, Zou X, Wang X and Fu Y 2022 *Plasma Sources Sci. Technol.* **31** 115002
- [65] Donkó Z and Petrović Z L 2006 *Japan. J. Appl. Phys.* **45** 8151–6
- [66] Kurihara M, Petrovic Z L and Makabe T 2000 *J. Phys. D: Appl. Phys.* **33** 2146–53
- [67] Bonham R A 1994 *Japan. J. Appl. Phys.* **33** 4157–64
- [68] Georgieva V 2006 Computer modeling of low-pressure fluorocarbon-based discharges for etching purposes *PhD Thesis* Universiteit Antwerpen (Belgium)
- [69] Denpoh K and Nanbu K 1998 *J. Vac. Sci. Technol. A* **16** 1201–6
- [70] Nanbu K and Kitatani Y 1995 *J. Phys. D: Appl. Phys.* **28** 324

- [71] Georgieva V, Bogaerts A and Gijbels R 2004 *Phys. Rev. E* **69** 026406
- [72] Nanbu K and Denpoh K 1998 *J. Phys. Soc. Japan* **67** 1288–90
- [73] Rauf S and Kushner M J 1997 *J. Appl. Phys.* **82** 2805–13
- [74] Denpoh K D K and Nanbu K N K 2000 *Japan. J. Appl. Phys.* **39** 2804
- [75] Schulenberg D A, Korolov I, Donkó Z, Derzsi A and Schulze J 2021 *Plasma Sources Sci. Technol.* **30** 105003
- [76] Brandt S et al 2016 *Plasma Sources Sci. Technol.* **25** 045015
- [77] Phelps A V and Petrovic Z 1999 *Plasma Sources Sci. Technol.* **8** R21
- [78] Buschhaus R, Prenzel M and von Keudell A 2022 *Plasma Sources Sci. Technol.* **31** 025017
- [79] Czarnetzki U, Schulze J, Schüngel E and Donkó Z 2011 *Plasma Sources Sci. Technol.* **20** 024010
- [80] Brinkmann R P 2007 *J. Appl. Phys.* **102** 093303
- [81] Raizer Y P and Allen J E 1991 *Gas Discharge Physics* vol 1 (Springer)
- [82] Georgieva V, Bogaerts A and Gijbels R 2003 *J. Appl. Phys.* **93** 2369–79
- [83] Proshina O V, Rakhimova T V, Rakhimov A T and Voloshin D G 2010 *Plasma Sources Sci. Technol.* **19** 065013
- [84] Descoedres A, Sansonnens L and Hollenstein C 2003 *Plasma Sources Sci. Technol.* **12** 152
- [85] Küllig C, Wegner T and Meichsner J 2015 *Phys. Plasmas* **22** 043515